Smart Structures and Systems, *Vol. 11, No. 6 (2013) 637-662*
DOI: http://dx.doi.org/10.12989/sss.2013.11.6.637

Structural health monitoring of the Jiangyin Bridge: system upgrade and data analysis

H.F. Zhou*[1], Y.Q. Ni[2] and J.M. Ko[2]

[1]*College of Architecture and Civil Engineering, Wenzhou University, Wenzhou, China*
[2]*Department of Civil and Environmental Engineering, The Hong Kong Polytechnic University, Hung Hom, Kowloon, Hong Kong*

(Received August 8, 2012, Revised December 15, 2012, Accepted January 8, 2013)

Abstract. The Jiangyin Bridge is a suspension bridge with a main span of 1385 m over the Yangtze River in Jiangsu Province, China. Being the first bridge with a main span exceeding 1 km in Chinese mainland, it had been instrumented with a structural health monitoring (SHM) system when completed in 1999. After operation for several years, it was found with malfunction in sensors and data acquisition units, and insufficient sensors to provide necessary information for structural health evaluation. This study reports the SHM system upgrade project on the Jiangyin Bridge. Although implementations of SHM system have been reported worldwide, few studies are available on the upgrade of SHM system so far. Recognizing this, the upgrade of original SHM system for the bridge is first discussed in detail. Especially, lessons learned from the original SHM system are applied to the design of upgraded SHM system right away. Then, performance assessment of the bridge, including: (i) characterization of temperature profiles and effects; (ii) recognition of wind characteristics and effects; and (iii) identification of modal properties, is carried out by making use of the long-term monitoring data obtained from the upgraded SHM system. Emphasis is placed on the verification of design assumptions and prediction of bridge behavior or extreme responses. The results may provide the baseline for structural health evaluation.

Keywords: structural health monitoring; performance assessment; environmental effect; system upgrade; long-span bridge

1. Introduction

The significance of implementing long-term structural health monitoring (SHM) systems for long-span bridges to secure structural and operational safety and issue early warnings on damage or deterioration prior to costly repair or even catastrophic collapse has been well recognized (Brownjohn 2007, Feng 2009). Successful implementation and operation of long-term SHM systems on bridges have been reported in many countries and regions (Wong and Ni 2009, Ou and Li 2010, Fujino and Siringoringo 2011, Yun *et al*. 2011). Early examples include the Great Belt Bridge in Demark (Andersen and Pedersen 1994), the Confederation Bridge in Canada (Cheung *et al*. 1997), the Tsing Ma Bridge in Hong Kong (Lau *et al*. 1999), the Commodore Barry Bridge in United States (Barrish *et al*. 2000), the Akashi Kaiyo Bridge in Japan (Sumitro *et al*. 2001), the

*Corresponding author, Professor, E-mail: mailtofei@wzu.edu.cn

http://www.techno-press.org/?journal=sss&subpage=8 ISSN: 1738-1584 (Print), 1738-1991 (Online)

Seohae Bridge in Korea (Kim *et al*. 2002), etc. To date, the implementation of a SHM system for a new long-span bridge seems becoming a common practice.

In Chinese mainland, the development of SHM systems for long-span bridges launched in 1994. The Xupu Bridge, a cable-stayed bridge with a main span of 590 m over the Huangpu River in Shanghai, is the first bridge being equipped with a SHM system (Shi *et al*. 2000). The Jiangyin Bridge with a main span of 1385 m over the Yangtze River in Jiangsu Province is another bridge being implemented with a long-term SHM system in the end of last century. As the first-generation bridge monitoring systems, they are of small scale with limited number of sensors. After years of operation, they are confronted with a problem on how to protect and maintain for long-term operation. Therefore, there exists a great demand for upgrading of the first-generation bridge monitoring systems in order to make them work properly as well as keep them updated with state-of-the-art SHM technologies.

Though implementations of SHM system have been reported worldwide, few studies are available on the upgrade of SHM system. In view of this, a SHM system upgrade project on the Jiangyin Bridge is reported in this study. As mentioned above, the bridge had been instrumented with a SHM system when completed in 1999. After operation for several years, it was found with malfunction in sensors and data acquisition units (DAUs), and insufficient sensors to provide necessary information for structural health evaluation. The SHM system has been upgraded by a joint venture of The Hong Kong Polytechnic University and Jiangsu Transportation Research Institute, which restored operation in June 2005. Structural health monitoring data have been continuously collected since then. This study presents SHM of the Jiangyin Bridge with emphasis on SHM system upgrade and data analysis. First, the upgrade of original SHM system for the bridge is discussed in detail. Especially, lessons learned from the original SHM system are applied to the design of upgraded SHM system right away. Then, performance assessment of the bridge by making use of the long-term monitoring data obtained from the upgraded SHM system is carried out. Specifically, the following analyses have been made: (i) characterization of temperature profiles and effects; (ii) recognition of wind characteristics and effects; and (iii) identification of modal properties. Emphasis is placed on the verification of design assumptions and prediction of bridge behavior or extreme responses.

2. The Jiangyin Bridge

The Jiangyin Bridge, as shown in Fig. 1, is a suspension bridge across the Yangtze River in Jiangsu Province, China. It connects the cities of Jingjiang in the north and Jiangyin in the south. It has a main span of 1385 m and two side spans of 336.5 m and 309.3 m each, making it the longest span suspension bridge in China at the time of its completion in 1999. The main span consists of 87 segments of flat streamlined steel box girder, which is an orthotropic structure composed of upper plates, lower plates, webs, transverse diaphragms and longitudinal U-shape troughs. The segment is 16 m in length typically, 3.0 m in height, and 36.9 m in width, carrying three traffic lanes and one pedestrian sidewalk in both directions. The steel box girder is supported on two sides (32.5 m apart) by hangers connected to the main cables. A total of 87 pairs of hangers (two hangers each pair) with an interval of 16 m typically are used on each side to suspend the steel box girder from the main cable. Wire rope is employed for hangers shorter than 10 m and parallel wire strand (PWS) for hangers longer than 10 m. Both types of hangers have a diameter of 80 mm. The main cable is made of prefabricated parallel wire strands (PPWS), which comprises 127 high

strength galvanized steel wires of 5.35 mm in diameter. The main span cable has 169 strands and the side span cable has 177 strands. Hence the main cables are around 0.9 m in diameter. The main tower is a reinforced concrete portal frame structure with two legs connected by three horizontal cross beams. Both towers have a height of 190 m, providing a 50 m high clearance for river navigation. On top of the tower is the saddle for carrying the main cable. When the saddle is factored in, the tower has a total height of 196 m. The Jiangyin Bridge is a milestone in the development of long-span bridges in Chinese mainland. It's the first long-span bridge of its kind to be designed in Chinese mainland as well as the first bridge with a main span exceeding 1 km in Chinese mainland. The bridge opened to traffic on September 28, 1999, in celebration of the 50th anniversary of PRC.

Fig. 1 The Jiangyin Bridge

3. Upgrade of structural health monitoring system

3.1 Original structural health monitoring system

The original SHM system comprised four kinds of sensors including 72 accelerometers, 14 elasto-magnetic (EM) sensors, 12 load pins, and a total station. The accelerometers were used for the measurement of bridge dynamic response and modal properties; the EM sensors for strand stress of the main cables near the anchorage; the load pins for tension forces of the hangers; the total station for global deflection (displacement) of the deck. The output from accelerometers and load pins was 4-20 mA current signals which were transferred via junction boxes into voltage signals as the input to DAUs. Both EM sensors and the total station output digital signals to DAUs through modulators/recorders with RS232 connectors. The DAU was a DART computer operated in Windows NT. A total of eight DAUs were employed to collect analogue/digital signals from neighboring sensors and digitize analogue signals. Five of them were located inside the deck, two inside the anchorage rooms, and one inside the northern tower. After transferring their analogue input signals into digital data, DAUs transmitted the collected data to the server in the administrative building through an Ethernet with 1 Mbps multi-mode (62.5-125 μm) fiber optic

cables. The core hardware was the fiber optic signal VNSwitch 900FX with SC connector.

After operation for several years, the original SHM system failed to function properly. Detailed field inspections carried out in 2004 showed that several DAUs ceased to work due to improper protection. A trouble-shooting analysis revealed the following problems: (i) The DAUs were not well protected against high temperature. A sealed cabinet for dustproof, moistureproof and waterproof, as shown in Fig. 2, had been designed for DAU. However, since some DAUs were located inside steel box girders where the temperature can be as high as 60^{o}C, the sealed cabinet caused the heat dispersing inside DAU very difficult and the high temperature made the electronic components of DAU prone to damage; (ii) The DAUs were insufficiently protected against lightning; (iii) The hard disk of the DART computer was used in a mode of on-line data storage, which made the hard disk work long-term without interruption and therefore shortened its service life. In addition, the EM sensors and load pins were also found with malfunction. In 2004, a joint venture of The Hong Kong Polytechnic University and Jiangsu Transportation Research Institute was commissioned by the bridge owner to upgrade the original SHM system.

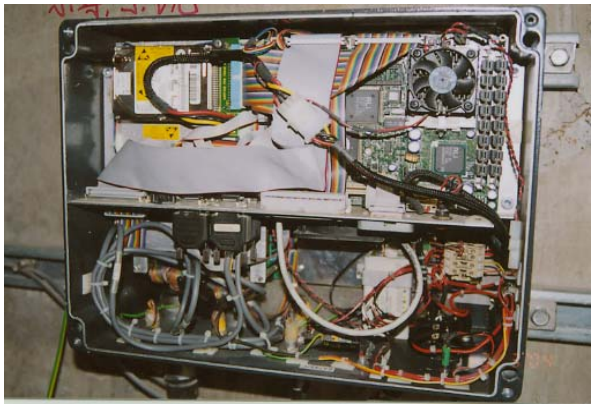

Fig. 2 Structure of DAU in original SHM system

3.2 Upgraded structural health monitoring system

3.2.1 Sensory system

The sensory system has been upgraded by repair/replacement of disordered sensors and installation of new types of sensors. The debugging of load pins and EM sensors were confronted with great difficulties. The load pins were tailor-made for the Jiangyin Bridge. But the manufacture has shut down production, making the debugging of the load pins difficult and expensive. It is therefore uneconomic to restore them. As a result, they were replaced by accelerometers. The EM sensors were not repaired because they were non-detachable from main cables. Neither were they replaced because they cannot be mounted on existing cables. The total station was replaced with the global positioning system (GPS) in order to capture a more complete bridge geometric configuration. It is now used for the measurement of deck deflection during routine inspections of the bridge. By so doing, a cross validation of the monitoring data from the GPS and the total station can be made. Benefiting from the good universality of accelerometers,

they were repaired and restored to work in the upgrade system except for some irreparable ones. From the debugging of sensors, a lesson learned is that the universality and replaceability should be more emphasized in the selection of sensors.

The intention of using 72 accelerometers in the original SHM system is unknown because the designer is out of contact. Herein, a lesson learned is that after-sale service should be more emphasized. In the upgraded SHM system, the location and direction of the accelerometer are determined to satisfy the modal identification of the bridge. To obtain finer mode shapes, it is desirable to use more accelerometers. However, a compromise between accuracy and economy has to be considered. More accelerometers require more dynamic data channels, which are usually more expensive. As a result, 35 repairable accelerometers have been restored to work. 15 accelerometers are fixed on the deck at the locations of 1/8, 1/4, 3/8, 1/2, and 3/4 main span. On each deck cross section, one accelerometer is placed at the center of the deck for the measurement of lateral acceleration and two accelerometers are respectively placed at the two edges of the deck for the vertical acceleration measurement. By so doing, lateral bending modes can be identified from the lateral accelerations, and vertical bending modes and torsional modes from the vertical accelerations. 12 accelerometers are mounted on the hangers. The 12 hangers originally equipped with load pins, which are believed to have the largest tension force, are selected. Eight accelerometers are installed on the main cables. One of the main cables is monitored at the locations of 1/4 and 1/2 main span, and mid side span. The other main cable is monitored at the location of 1/4 main span only. At each measurement point, two accelerometers are employed to measure the vertical and lateral accelerations. Usually, the boundary conditions of the main cable are very complicated due to the presence of a large amount of hangers, which are equivalent to its constraints. The complexity of the boundary conditions poses a great challenge to the extraction of mode shapes of the main cable, especially for high order modes. Without the help of mode shape, the judgment of a true or false mode is difficult, especially local modes of the main cable. In view of this, the accelerometers on the main cables are not designed for identifying their mode shapes. Rather, they are designed for obtaining the fundamental modal frequency of the main cable which is essential to the calculation of cable force. In addition, they may also help validate some global modes (appear both on the deck and on the cable) of the bridge.

Usually, three categories of parameters are monitored in a bridge SHM system: (i) loading sources, such as wind, temperature, traffic, earthquake, and so on; (ii) bridge characteristics, which are mainly dynamic properties; and (iii) bridge responses, like strain, cable force, etc. Therefore, new types of sensors have also been installed in order to provide more information for structural health evaluation, including anemometers, displacement transducers, GPS, and fiber optic strain and temperature sensors. Two tri-axial ultrasonic anemometers are placed at the tower top and the deck in the mid main span for wind speed and direction measurement. Eight GPS receivers are deployed to capture the bridge geometric configuration, with two on the top of the towers and the other six at the two edges of the deck at the locations of 1/4, 1/2, and 3/4 main span. Four displacement transducers are used to measure the longitudinal movement of expansion joint (two for each expansion joint). 116 fiber optic sensors are attached to the deck in the main span for strain and temperature measurement, including 72 fiber optic sensors on nine equidistant cross-sections (eight on each section) for measurement of longitudinal strain, eight on the mid span cross-section for transverse strain measurement, and 36 on nine equidistant cross-sections (four on each section) for temperature measurement. Fig. 3 shows the deployment of sensors on the Jiangyin Bridge. The upgraded SHM system has about 170 sensors. The sampling rates of sensors are summarized in Table 1.

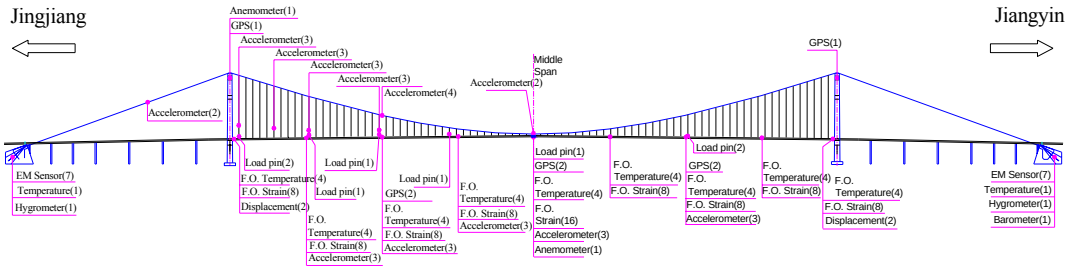

Fig. 3 Deployment of sensors on the Jiangyin Bridge

Table 1 Sampling frequency of sensors

No.	Sensor	Sampling frequency (Hz)
1	Tri-axial ultrasonic anemometer	1
2	GPS	1
3	Fiber optic strain and temperature sensor	1
4	Displacement transducer	50
5	Accelerometer	50

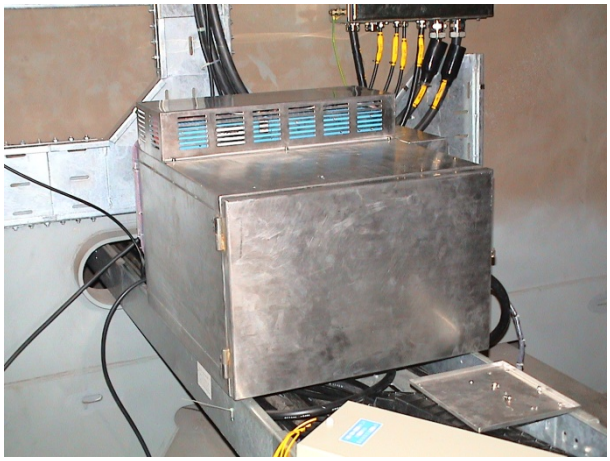

Fig. 4 Stainless steel cabinet for protection of DAU

3.2.2 Data acquisition and transmission system

The data acquisition and transmission system has been upgraded by replacement of DAUs and data transmission network. In the authors' opinion, the malfunction of DAU is the direct cause of the breakdown of original SHM system. Recognizing this, utmost care has been taken of the

design of DAU. The performance of DAU is guaranteed from the fountainhead with the use of industrial personal computer (IPC), which is capable of long term reliable work. Furthermore, an elaborate protection system has been designed for the DAU. A stainless steel cabinet shown in Fig. 4 has been fabricated to house the DAU and to protect it from temperature, dust, humidity, and lightning. A temperature control system has been settled inside the cabinet to accommodate severe temperature conditions inside the steel box girders, and an isolation transformer is adopted at each DAU to protect it from lightning. To take full advantage of the state-of-the-art network technology, the original 1 Mbps multi-mode fiber optic network has been replaced by 100 Mbps single-mode fiber optic network. The DAUs on the bridge are connected with the server in the control room with this fiber optic network. All DAUs are synchronized with the server with the help of a pulse generator on the server. By sending a pulse signal from the server to the DAUs through the fiber optic network every five minutes, the synchronization of the DAUs is fulfilled.

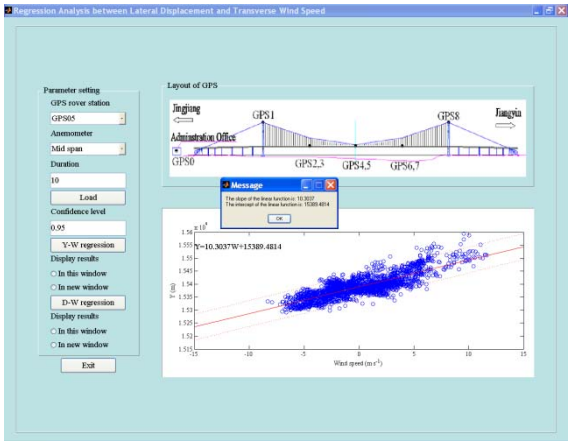

Fig. 5 User interface for advanced data analysis software

3.2.3 Software systems

New software systems have been developed for data acquisition, transmission, display, preprocessing, and advanced analysis. One software system developed under LabVIEW environment has been embedded in DAUs for the acquisition, transmission, display, preprocessing, and archiving of raw data. Emphasis is placed on the remote control of data sampling settings, on-line display and animation of raw data and preprocessed results. Although the DAU is well protected, occasional malfunction of DAU is inevitable. Therefore, on-line display and animation of raw data is designed for the DAU to facilitate the debugging of DAU. In daily operations, however, the on-line display and animation of raw data is shut down. The raw data are transmitted to the server in the control room for subsequent data processing. Another software system for advanced data analysis carried out on the server has also been developed with the commercial software MATLAB (Zhou *et al*. 2007). It consists of eight modules: (i) serviceability assessment, including factors of deflection, expansion joint displacement, and vibration; (ii) analysis of wind characteristics, such as mean wind speed and direction, wind speed profiles, turbulence intensity, gust factor, wind spectrum, etc.; (iii) prediction of extreme deck lateral displacement based on

wind and displacement data; (iv) assessment of expansion joint using temperature and expansion joint displacement data; (v) modeling of modal variability with back-propagation neural network technique; (vi) structural damage alarming with auto-associative neural network technique; (vii) safety index evaluation of bridge components based on reliability analysis of strain data; and (viii) analysis of fatigue life expectance using strain data. To relief end-users from abstruse algorithms, user interfaces have also been devised with MATLAB GUI. To make them easy to use, different data analysis modules are designed with similar user interfaces. Generally, the window is divided into three areas. The left of the window is used for the input of analysis parameters. The upper right window is used for the demonstration of sensor layout, and the lower right window for the visualization of analysis results. Pop-up windows are also designed for the display of prompt messages and/or warning messages. An example of the user interface is presented in Fig. 5.

4. Monitoring data analysis and performance assessment

The upgraded SHM system commenced trial operation in June 2005. Since then, structural health monitoring data have been continuously collected. Making use of the long-term monitoring data, performance assessment of the Jiangyin Bridge is carried out with the advanced data analysis software.

4.1 Characterization of temperature profiles and effects

As mentioned earlier, nine equidistant cross-sections in the main span are instrumented with fiber optic temperature sensors. On each cross-section, two fiber optic temperature sensors are attached to the upper deck plate and two the bottom deck plate, as shown in Fig. 6. The deck effective temperature and differential temperature are first computed from the temperatures in a deck cross-section for representing the temperature profiles in the deck. Then, the thermal movement of expansion joint is studied and the displacement-temperature correlation model is formulated for design verification as well as extreme value prediction. Finally, the temperature-induced strain variability is explored and the strain-temperature correlation model is established for the quantitative estimation of thermal strain.

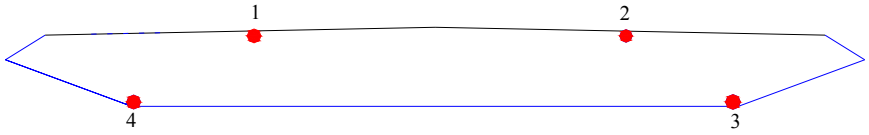

Fig. 6 Layout of fiber optic temperature sensors on the deck cross section

4.1.1 Profiles of deck effective temperature

Temperature in a bridge deck cross-section can be divided into effective temperature and differential temperature. The former is an average of temperatures distributed over the cross-section, which accounts for the thermal movement of bridge deck; while the latter refers to

temperature differences between the top surface and other levels in the cross-section, which results in supplementary internal axial forces and bending moments when the section ends are restrained (Maes *et al*. 1992). According to the definition, the effective temperature can be expressed as

$$T_e = \frac{1}{A}\iint_A T(x,y)dxdy \tag{1}$$

where A is the area of the cross-section; $T(x,y)$ is the temperature distribution over the cross-section. When measuring the temperature on a cross-section, the temperature sensors are always installed at a number of discrete locations of the cross-section. By dividing the cross-section into an appropriate number of sub-areas and assuming identical temperature in each sub-area, the effective temperature can be obtained by weighted average of the temperatures measured at all sub-areas, where the weighting is the ratio of each sub-area to the total area of the cross-section. That is

$$T_e = \sum_{i=1}^{k} \frac{A_i}{A}\overline{T_i} \tag{2}$$

where A_i is the ith sub-area; $\overline{T_i}$ is the measured temperature at the ith sub-area; and k is the number of sub-areas divided for the cross-section.

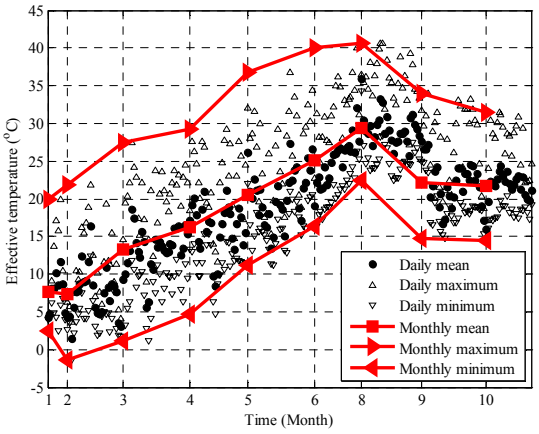

Fig. 7 Deck effective temperature in 2006

Fig. 7 shows the statistics of deck effective temperature in the year of 2006, in which both daily and monthly statistics are presented. An apparent annual variation pattern of the effective temperature is observed. The overall uptrend is obvious in the first half year and the overall downtrend is clear in the second half year. The highest effective temperature in this year was 40.60 ^{o}C recorded on August 13 and the lowest effective temperature was -1.33^{o}C on February 3. Fig. 8 zooms in the effective temperature in the month of June with hourly statistics being plotted.

Besides the overall uptrend of the effective temperature, obvious daily cyclic variation pattern is also found. The effective temperature usually reaches a minimum around 7 AM and a maximum around 3 PM in each day. The differences between hourly maximum, mean and minimum are small, which indicate the steady variation characteristics of effective temperature. Fig. 9 presents the histogram of the daily variation range of effective temperature. The maximum day/night difference of effective temperature is 17.31^{o}C on March 19. Most of the day/night differences of effective temperature are in the range of 11~14^{o}C. The temperature difference in a deck cross section, which is the difference between the maximum and minimum temperatures at the same time, is also calculated. Fig. 10 shows the histogram of hourly averaged temperature differences. It is seen that the temperature differences in the deck cross section are mostly in the range of 1~3^{o}C.

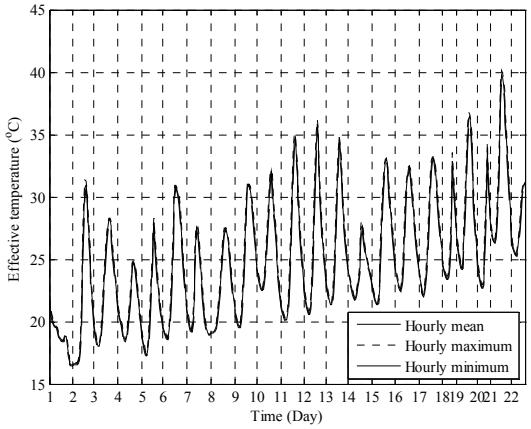

Fig. 8 Deck effective temperature in June 2006

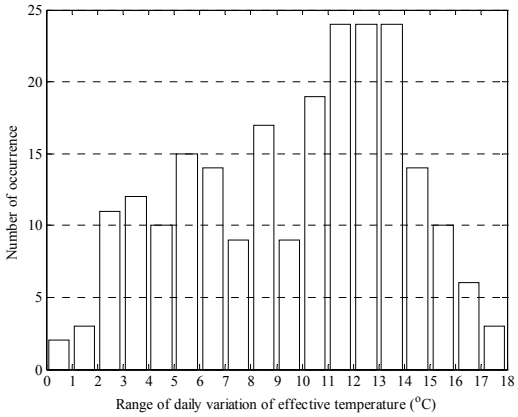

Fig. 9 Daily variation range of deck effective temperature in 2006

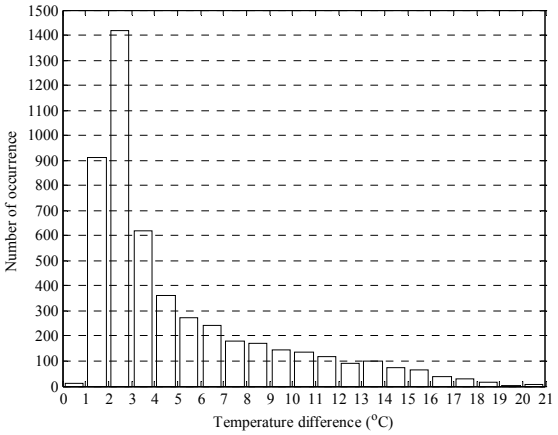

Fig. 10 Histogram of hourly averaged temperature differences

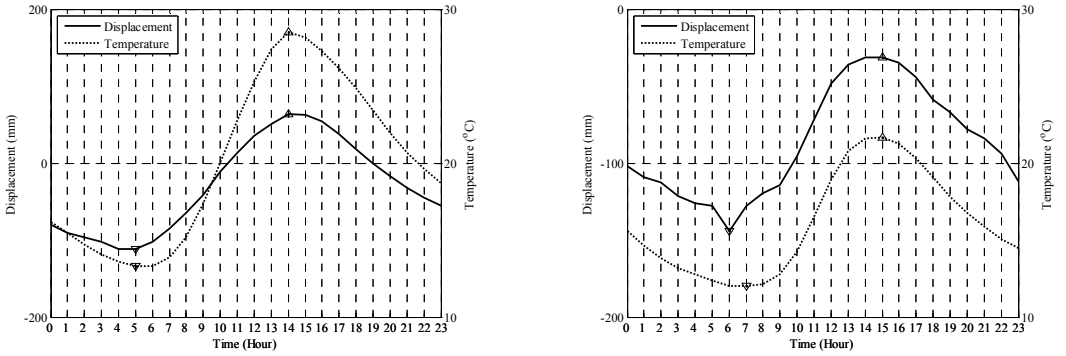

(a) Time history on May 03 2006 (b) Time history on March 26 2006

Fig. 11 Examples of displacement-temperature time history

4.1.2 Pattern of thermal movement

The thermal movements of expansion joints, due to temperature fluctuations, are an important consideration in the bridge design. For the Jiangyin Bridge, both expansion joint displacement and deck temperature are monitored. From the one-year monitoring data, it is observed that the expansion joint displacement and deck effective temperature generally exhibit a linear relationship. Similar observations have also been found on the Ting Kau Bridge in Hong Kong (Ni *et al*. 2007a).

However, the linear relationship is sometimes affected by traffic, especially in the time intervals with heavy vehicle passes. In addition, no significant thermal inertial effect between them is observed. Fig. 11 shows the time histories of expansion joint displacement and deck effective temperature. In Fig. 11(a), a good correlation between them is observed. The expansion joint displacement expands as the deck effective temperature increases and contracts as it decreases. In

Fig. 11(b), the displacement-temperature relationship is severely polluted with the occurrence of an extra valley in the displacement in the time intervals of 3~7 AM. In other time intervals, however, the correlations between them remain good. As over-loading vehicles are permitted to pass the bridge in the time intervals of 0~7 AM, which roughly coincides with the time at the occurrence of the extra valley, the observed valley in the displacement is therefore attributed to the passes of over loading vehicles.

Correlation models between expansion joint displacement and deck effective temperature are established for design verification as well as extreme value prediction. First, displacement and temperature data are selected for model formulation. Since traffic is not monitored, the traffic effect is roughly eliminated by selecting only the displacement unaffected by heavy vehicle passes. Recalling the observed linear displacement-temperature relationship, linear regression analysis is then employed to formulate their correlation model. The least-square method is employed to obtain the regression coefficients. Fig. 12 shows the measured and fitted relationships between them. The regression functions are expressed as

$$D = 10.90T - 245.35\,(\text{mm}) \quad \text{at Jingjiang tower} \tag{3a}$$

$$D = 9.89T - 79.73\,(\text{mm}) \quad \text{at Jiangyin tower} \tag{3b}$$

where D is the expansion joint displacement; T is the deck effective temperature. Design verification is performed by making use of Eq. (3). Assume that the thermal movement is symmetrical to the mid span, the expansion length is determined to be approximately 692.50 m for both expansion joints. The thermal expansion coefficient is thus estimated as 15.74×10^{-6} m/^{o}C and 14.27×10^{-6} m/^{o}C, respectively, which is higher the design value of 12.00×10^{-6} m/^{o}C. By presenting the observed maximum and minimum deck effective temperature into Eq. (3), which is respectively 40.60^{o}C and –1.33^{o}C, the range of expansion joint displacement induced by temperature variation is computed to be 660 mm and 598 mm for the expansion joint at Jingjiang and Jiangyin tower, respectively.

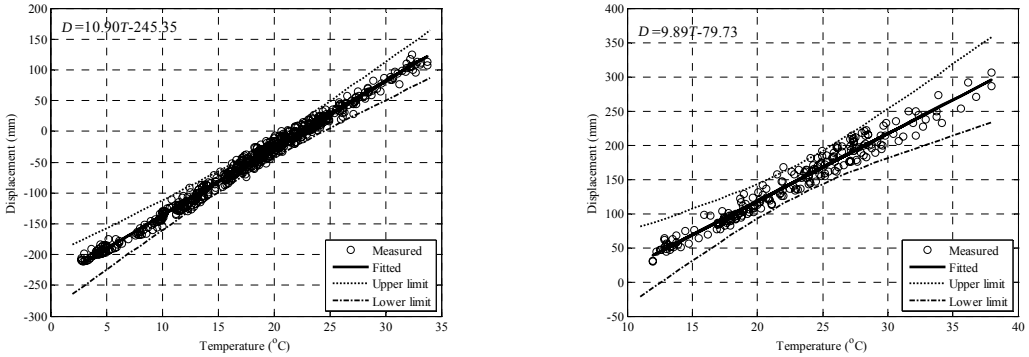

(a) Expansion joint at Jingjiang tower (b) Expansion joint at Jiangyin tower

Fig. 12 Relationships between expansion joint displacement and deck effective temperature

4.1.3 Pattern of thermal strain

Despite thermal movements in the bridge are generally unnoticeable, thermal strain are actually induced in structural components. From the strain and temperature monitoring data, there is evidence of correlation between them. For the Jiangyin Bridge, the following findings are obtained: (i) strain and temperature generally exhibit a linear relationship; (ii) thermal inertial effect exists in the strain-temperature relationship and it seemingly varies with temperature; (iii) significant effect of traffic on the strain is also observed in the time intervals with heavy vehicle passes. Fig. 13 illustrates the time histories of strain and effective temperature. As it is seen from Fig. 13(a), the decrease of effective temperature may change the nature of strain from compression to tension and reduce/increase the magnitude of compression/tension strain, and vice versa. In the morning, the strain lags behind the effective temperature about two hours. In the afternoon, however, the time lag between them shortens to about one hour. In Fig. 13(b), an extra valley is also found in the strain in the time intervals of 3~7 AM, which is similar to the displacement-temperature relationship. Again, it is attributed to the passes of heavy vehicles. Similar thermal inertial effect is also observed in the strain affected by heavy vehicles passes.

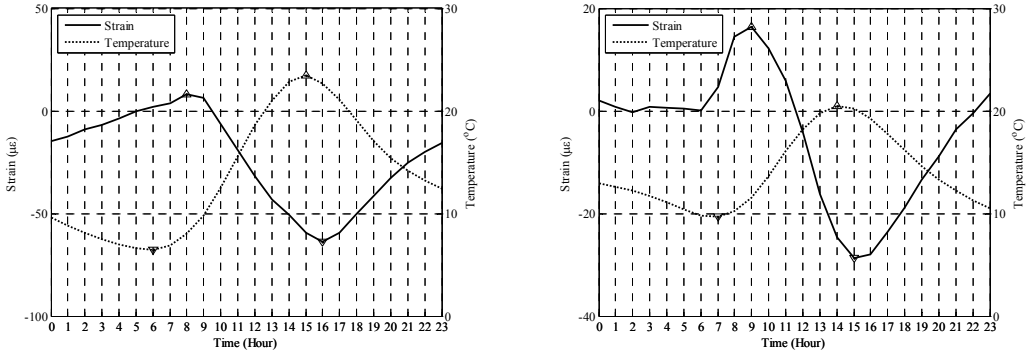

(a) Time history on March 19 2006 (b) Time history on March 23 2006

Fig. 13 Examples of time history of strain and effective temperature

Correlation models between strain and temperature are formulated to quantify the temperature effect on the strain. First, strain and temperature data are selected for model setup by picking out strain unaffected by heavy vehicle passes. Recognizing the observed linear strain-temperature relationship, linear regression analysis is then employed to formulate their correlation model. Again, the least-square method is used to obtain the regression coefficients. The optimal correlation model is found through the selection of appropriate temperature type and location, and the setting of appropriate time lag. Both the temperature at a specific monitoring point and the deck effective temperature are used as the input variable with the intention to explore the effects of temperature type and location on the strain-temperature relationship. As a result, a total of five input cases are considered, including four individual temperatures at each monitoring point and one deck effective temperature. The thermal inertial effect is simulated by the time lag between strain and temperature. Different time lag cases are simulated. The optimal strain-temperature

correlation model is considered the one that generates the smallest variance of residuals. The results show that the model with the input of temperature that is closest to the strain monitoring point, and one-hour time lag in between them produces the smallest variance of residuals. It is also found that the use of effective temperature generates models worse than the use of temperatures at the upper deck plate but better than the use of temperatures at the bottom deck plate, which validates the average meaning of the effective temperature. In addition, the model with one-hour time lag between strain and temperature always generates the smallest residual among the models which have a same input variable.

Fig. 14 presents the measured and fitted relationships between strain and temperature. It is seen that one unit increase in temperature will result in about 2.47 με decrease in strain. Recall that the maximum day/night difference of the effective temperature is 17.31°C, the temperature alone will cause a maximum variation of 42.85 με in the strain within a single day. The upper and lower bounds with a confidence level of 0.95 are also illustrated in Fig. 14. All monitored data fall within the bounds.

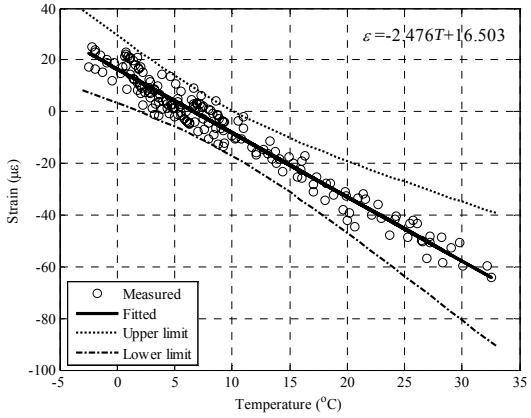

Fig. 14 Relationships between strain and temperature

4.2 Recognition of wind characteristics and effects

Two tri-axial ultrasonic anemometers are placed on the tower top and at the deck in the mid main span for the measurement of wind speed and direction. The anemometer on the tower top breaks down occasionally, resulting in the loss of monitoring data in some time intervals. The possible reason is that the ultrasonic anemometer may not be fit for the measurement of high wind speed since the wind speed on the tower top is much higher than that at the deck level. The wind data are first analyzed to obtain wind characteristics, including: (i) mean wind speed and direction, (ii) wind speed profiles, (iii) turbulence intensity, (iv) gust factor, and (v) wind spectrum. In the mean while, verification of design assumptions and rules of thumb are made. After that, the wind-induced deck lateral displacement is studied and the correlation model is established for the quantitative estimation of wind-induced deck lateral displacement.

4.2.1 Statistics of mean wind speed and direction

Tables 2 and 3 summarize the maximum mean wind speeds recorded at the deck level and on the tower top, respectively. As it is seen, the wind speeds at the bridge site over these years were relatively mild. The maximum 10-minute mean wind speed is 18.78 m/s at the deck level, which is much lower than the design value of 41.00 m/s as specified in the "Wind-resistant Design Specification for Highway Bridges" (Ministry of Transport of the People's Republic of China 2004). Due to the malfunction of the anemometer on the tower top, statistics of the wind speed on the tower top is not comprehensive. The recorded maximum 10-minute mean wind speed on the tower top is 20.06 m/s, which is also lower than the design value.

Table 2 Maximum wind speeds recorded at the deck level

Month	1-minute mean (m/s)	10-minute mean (m/s)	60-minute mean (m/s)
July 2005	14.64	13.31	12.22
August 2005	21.45	18.78	16.67
January 2006	10.80	9.53	8.87
March 2006	16.97	15.15	10.30
April 2006	15.22	12.25	11.18
May 2006	18.82	16.20	14.65
June 2006	11.09	9.80	9.06
July 2006	9.73	7.37	7.02
August 2006	9.85	7.05	5.82
September 2006	8.63	8.00	7.13
October 2006	9.47	8.77	7.46
November 2006	16.32	14.76	13.77
January 2007	11.22	9.33	8.35
February 2007	11.41	10.49	9.51
March 2007	16.73	15.99	14.09
April 2007	15.58	13.42	12.54
May 2007	15.18	13.48	12.02
June 2007	14.60	13.24	11.67
July 2007	13.75	11.39	10.74

Over the past few years, only one typhoon "Matsa" was measured at the bridge site. Fig. 15 shows the 10-minute mean wind speed and direction before, during, and after typhoon "Matsa" (from August 5 to August 7 2005). As it is seen, the maximum wind speed occurred when typhoon

"Matsa" attacked the bridge. The wind mainly blew from southeast during typhoon "Matsa". It is interesting to see that the maximum wind speed occurred when the wind direction started to change from southeast to south (around 2 AM, August 7 2005).

Table 3 Maximum wind speeds recorded on the tower top

Month	1-minute mean (m/s)	10-minute mean (m/s)	60-minute mean (m/s)
January 2006	13.6	12.21	11.33
August 2006	16.96	14.83	12.53
September 2006	15.9	13.97	13.01
October 2006	14.66	13.75	11.05
November 2006	18.11	17.79	16.96
January 2007	17.44	15.82	14.96
February 2007	17.64	17.24	15.12
March 2007	22.91	20.06	18.26
April 2007	21.07	19.21	18.16
May 2007	21.37	19.65	18.09
June 2007	20.34	18.45	16.56

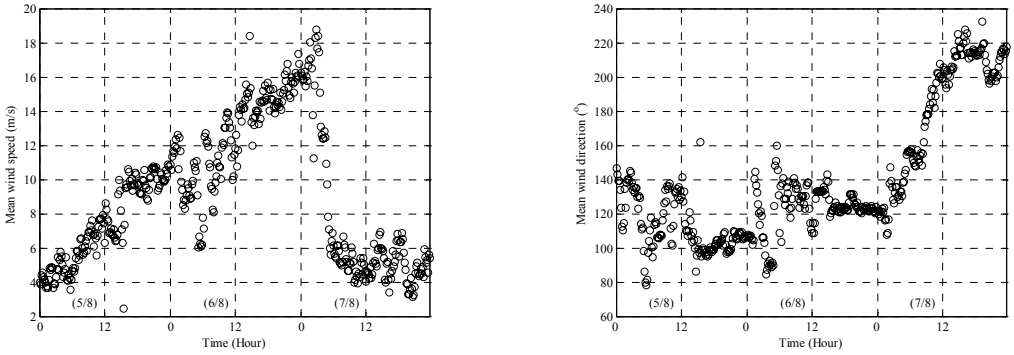

(a) Mean wind speed (b) Mean wind direction

Fig. 15 Mean wind speed and direction before, during, and after typhoon "Matsa"

4.2.2 Profiles of wind speed

Wind speed profiles may be approximated by the power law, i.e.

$$\frac{\overline{U}_{z_1}}{\overline{U}_{z_2}} = \left(\frac{z_1}{z_2}\right)^{\alpha} \tag{4}$$

where $\overline{U}_{z_1}$, $\overline{U}_{z_2}$ is the mean wind speed at height z_1 and z_2, respectively; α is the terrain roughness. Usually, the terrain roughness of a specific site is not known a prior. For design purposes, some design codes classify the terrain into several categories and designate a terrain roughness for each category. For the Jiangyin Bridge, wind speeds at the levels of deck and tower top are measured. Making use of the power law, the terrain roughness can be estimated. First, a linear regression model with a unit slope is established between the logarithms of the mean wind speeds at the two levels by the least-squares method. The terrain roughness is then estimated from the fitted linear regression model. As only high wind speeds are interested, records with more than 10.00 m/s 10-minute mean wind speeds are used in this analysis. As a result, the terrain roughness is estimated as 0.25, which is close to the proposed value of 0.22 in the "Wind-resistant Design Specification for Highway Bridges" (Ministry of Transport of the People's Republic of China 2004).

4.2.3 Statistics of turbulence intensity

Turbulence intensity is defined as the ratio of standard deviation of fluctuating wind to mean wind speed for a given duration. It is an important parameter in the determination of wind-induced dynamic response of structures, which reflects the intensity of fluctuating wind. For flat terrain, the longitudinal turbulence intensity may also be approximated by (Dyrbye and Hansen 1997)

$$I_u(z) = \frac{1}{\ln(z / z_0)} \tag{5}$$

where z is height; z_0 is surface roughness length. The surface roughness length at the Jiangyin Bridge site is 0.30 m, by matching the terrain with Category C in the "Wind-resistant Design Specification for Highway Bridges" (Ministry of Transport of the People's Republic of China 2004). Using Eq. (5), the longitudinal turbulence intensity of 18.63% at the deck level and 15.42% on the tower top are estimated.

Table 4 summarizes the statistics of turbulence intensity of one-hour duration at the deck level and on the tower top, respectively. Only turbulence intensities under more than 10.00 m/s hourly mean wind speed are considered, resulting in 120 samples at the deck level and 543 samples on the tower top. The turbulence intensity at the deck level is much higher than that on the tower top, which conforms to Eq. (5). The average longitudinal turbulence intensity at the deck level is 19.14%, which is close to the estimated value of 18.63%. The average lateral turbulence intensity at the deck level is 16.38%. The mean of lateral to longitudinal turbulence intensity at the deck level is 0.89, conforming to the proposed value of 0.88 in the "Wind-resistant design specification for highway bridges" (Ministry of Transport of the People's Republic of China 2004). The average longitudinal turbulence intensity on the tower top is 13.30%, which is a little bit lower than the estimated value of 15.42%. The average lateral turbulence intensity on the tower top is 9.12%. The mean of lateral to longitudinal turbulence intensity on the tower top is 0.73, which is very close to the proposed value of 0.75 at a height of about 100~200 m above homogeneous terrain (Dyrbye

and Hansen 1997).

Table 4 Statistics of turbulence intensity of one hour duration

Level	Turbulence intensity	Maximum	Minimum	Mean
Deck	I_u (longitudinal)	51.23%	11.93%	19.14%
	I_v (transverse)	41.86%	9.56%	16.38%
	I_v/I_u	1.74	0.41	0.89
Tower top	I_u (longitudinal)	52.24%	2.08%	13.30%
	I_v (transverse)	49.45%	1.55%	9.12%
	I_v/I_u	2.16	0.22	0.73

4.2.4 Statistics of gust factor

The gust factor $G(t)$ is often defined as the ratio of the gust speed of gust duration t to the hourly mean wind speed. As gusts are the results of the turbulent agitation of the wind, the gust factor is often related to the turbulence intensity. In general, gust factors can be calculated as a function of turbulence intensity and the gust period. Choi (1983) presented the following expression based on wind data measured from several places in Hong Kong

$$G(t) = 1 + 0.62 I_u^{1.27} \ln(3600/t) \tag{6}$$

A simplified expression proposed by Cook (1985) is given as follows

$$G(t) = 1 + 0.42 I_u \ln(3600/t) \tag{7}$$

Table 5 provides statistics of the 3-second gust factors. Again, only records with more than 10 m/s hourly mean wind speed are included in this analysis. The 3-second gust factor at the deck level varies between 1.24 and 3.01 with a mean of 1.53. The gust factor on the tower top is smaller overall. It falls in a range of 1.05 to 1.91 with a mean of 1.31. Fig. 16 shows the measured relationship between 3-second gust factor and turbulence intensity. The relationships expressed by Eqs. (6) and (7) are also presented. At the deck level, an overall increase trend is observed; however, it is much dispersed when the turbulence intensity increases. Eq. (6) fits the measured relationship a little bit better than Eq. (7). The root mean square error predicted using Eqs. (6) and (7) is 0.175 and 0.190, respectively. Using Eq. (7), the gust factor is overestimated in the lower range of turbulence intensity, while it is underestimated in the upper range of turbulence intensity. On the tower top, the measured relationship is much more uniform. It is also obvious that the slope of the relationship between the gust factor and turbulence intensity is less than one. Therefore, both expressions overestimate the gust factor. The root mean square error predicted using Eqs. (6) and (7) is almost the same, both are 0.139.

Table 5 Statistics of 3-second gust factors

3-Second gust factor	Maximum	Minimum	Mean
Deck level	3.01	1.24	1.53
Tower top	1.91	1.05	1.31

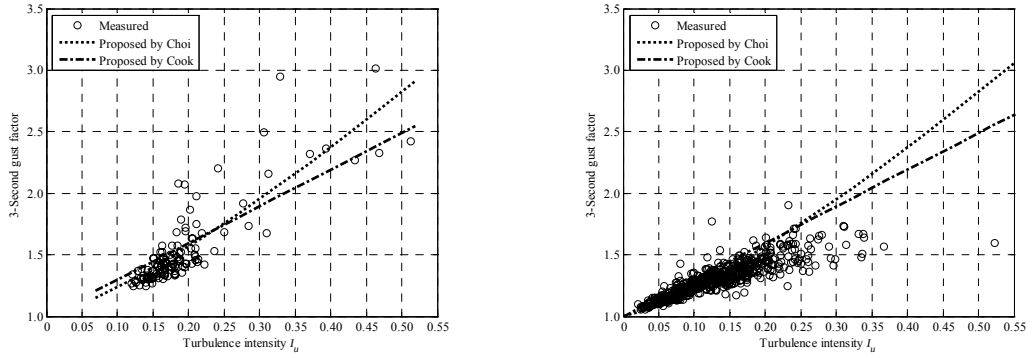

(a) Deck level (b) Tower top

Fig. 16 Relationships between 3-second gust factor and turbulence intensity

4.2.5 Pattern of wind spectrum

The auto-spectrum of turbulence describes the wind energy distribution over frequency. It will significantly affect the wind-induced dynamic response of a structure. For structural design purposes, several expressions for wind spectrum have been suggested. In the "Wind-resistant Design Specification for Highway Bridges" (Ministry of Transport of the People's Republic of China 2004), Kaimal spectrum is adopted, which is expressed as

$$\frac{nS_u(n)}{u_*^2} = \frac{200f}{(1+50f)^{5/3}} \tag{8a}$$

$$\frac{nS_v(n)}{u_*^2} = \frac{15f}{(1+9.5f)^{5/3}} \tag{8b}$$

where n is the frequency; $S_u(n)$, $S_v(n)$ is the spectrum of longitudinal and lateral wind fluctuating component, respectively; u_* is the friction velocity; and $f = \frac{nz}{\overline{U}}$ is a nondimensional quantity known as the Monin coordinate. Simiu and Scanlan (1996) presented similar equations as

$$\frac{nS_u(n)}{u_*^2} = \frac{105f}{(1+33f)^{5/3}} \tag{9a}$$

$$\frac{nS_v(n)}{u_*^2} = \frac{17f}{(1+9.5f)^{5/3}} \tag{9b}$$

Fig. 17 illustrates the longitudinal and lateral auto-spectra of the wind speed on the tower top during non-typhoon period (at 12 PM, 30 August 2006). The auto-spectra are computed using samples of one-hour duration. The Kaimal, and Simiu and Scanlan spectra are also plotted for comparison. It is seen that the two empirical spectra are similar and both of them match favorably with the measured spectra during non-typhoon period. It is also observed that the peak or most dominant fluctuating components mostly occurred when Monin coordinate is less than 0.20. As described below, the fundamental modal frequency of the Jiangyin Bridge is more than 0.05 Hz. With a mean wind speed of 6.21 m/s in this hour, the corresponding Monin coordinate is more than 1.58. Therefore, the peak frequencies of wind did not coincide with the modal frequencies of the bridge. As far as the wind spectrum during typhoon "Matsa" is concerned, both empirical spectra do not match well with the measured spectra.

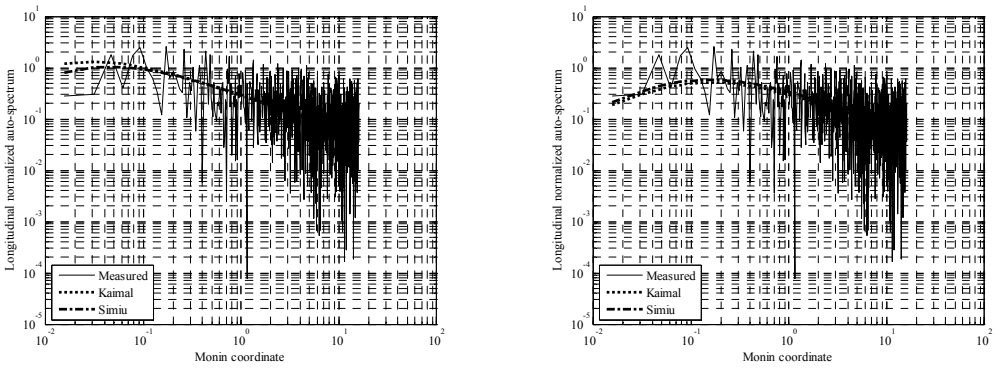

(a) Longitudinal spectrum (b) Lateral spectrum

Fig. 17 Wind auto-spectra on the tower top during non-typhoon period

4.2.6 Pattern of wind induced displacement

Similar to temperature, which is the main source of the deck longitudinal displacement, wind is found to be the main factor causing the deck lateral displacement from the monitoring data of wind and displacement. Fig. 18 illustrates time histories of the deck Y-coordinate (lateral displacement) and transverse wind speed at the deck level. The transverse wind speed is obtained by decomposing the measured wind speed into transverse and longitudinal components, and the 10-minute mean is shown. On the whole, the lateral displacement varies in step with the transverse wind speed, indicating wind mainly accounts for the deck lateral displacement. Therefore, linear regression models are formulated to quantify the wind effect on the deck lateral displacement. The parameters of the regression models obtained by the least-square method are summarized in Table 6, including the slope α, intercept β, and variance of residuals $\hat{\sigma}$. It is seen that the regression models at the two sides of a deck cross section is almost the same. At the mid span, one unit change in wind speed will make the deck move about 10 mm laterally. With the maximum design

wind speed of 41.00 m/s, it is predicted that the maximum deck lateral displacement at the mid span will approximate 423 mm. Fig. 19 sketches the deformed shape of the bridge deck in lateral direction under a unit change of wind speed. The deck lateral displacement induced by a unit change of wind speed is obtained from the linear regression model, which is actually the slope of the linear regression model. The predicted lateral displacements at the two edges of a deck cross section are averaged and then plotted in Fig. 19.

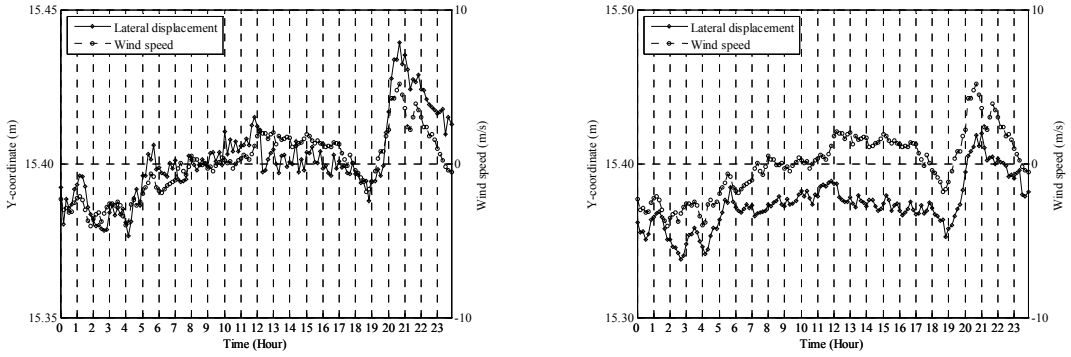

(a) 1/4 main span (b) Mid span

Fig. 18 Examples of time history of deck Y-coordinate and transverse wind speed

Table 6 Parameters of linear regression models between deck Y-coordinate and transverse wind speed at deck level

Y-coordinate	α	β	$\hat{\sigma}$ ($\times 10^{-3}$ m)
1/4 main span	7.99×10^{-3}	15.41	14.03
1/4 main span	7.71×10^{-3}	-15.34	13.29
Mid span	10.55×10^{-3}	15.38	17.10
Mid span	10.08×10^{-3}	-15.40	16.43
3/4 main span	8.19×10^{-3}	15.35	15.26
3/4 main span	7.82×10^{-3}	-15.40	14.20

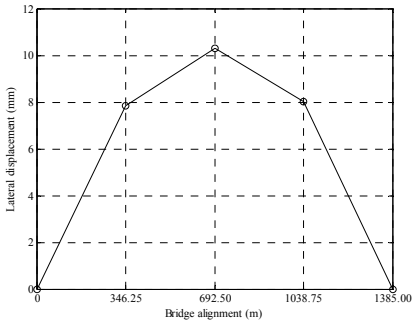

Fig. 19 Laterally deformed shape of bridge deck due to a unit change of wind speed

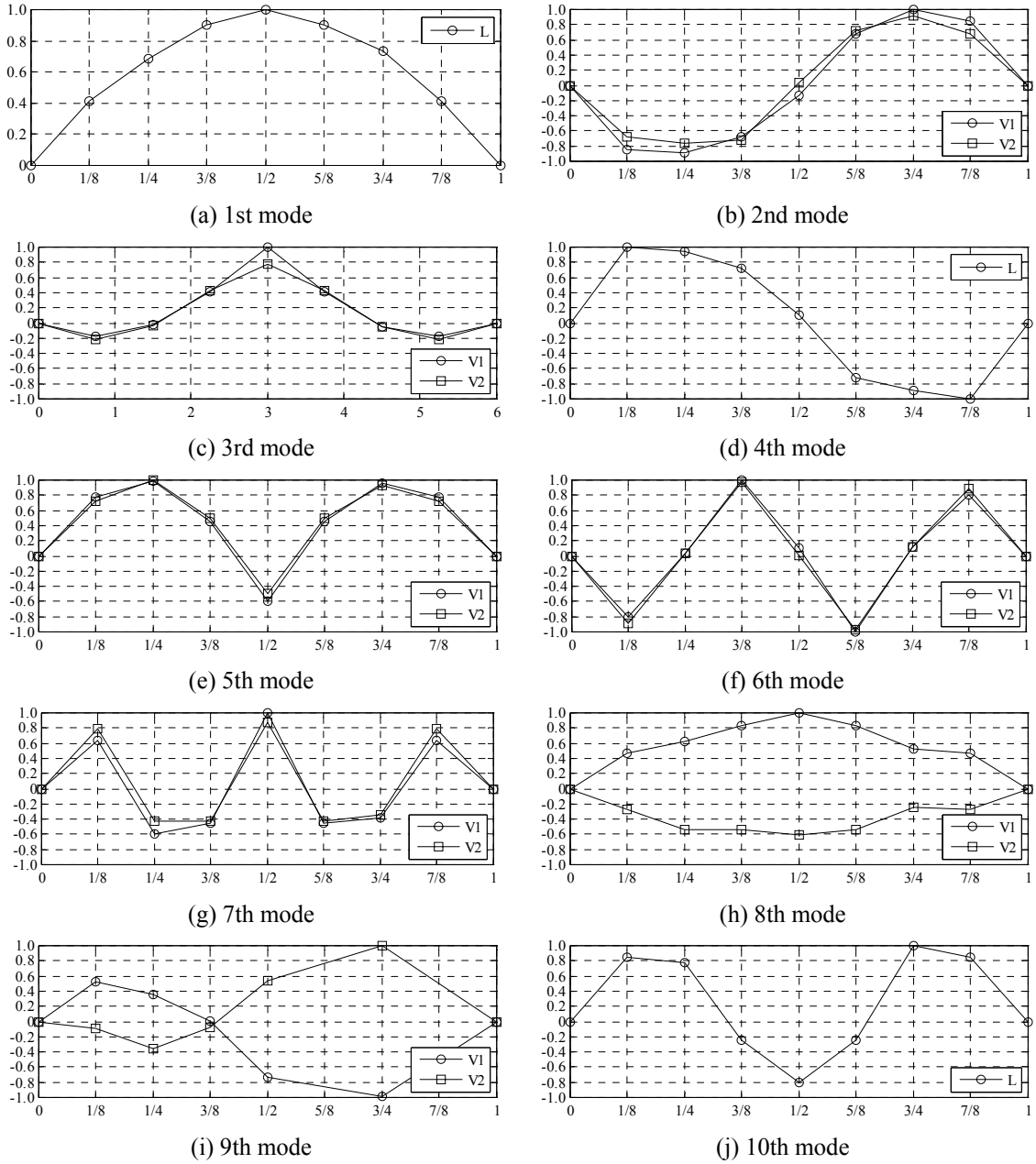

(a) 1st mode (b) 2nd mode

(c) 3rd mode (d) 4th mode

(e) 5th mode (f) 6th mode

(g) 7th mode (h) 8th mode

(i) 9th mode (j) 10th mode

Fig. 20 Identified shapes of the first 10 modes

4.3 Identification of modal properties

Vibration-based structural damage detection is the fastest growth area in the field of SHM (Doebling et al. 1998, Sohn et al. 2004). The philosophy is rather simple: the occurrence of structural damage or deterioration will change the physical properties of a structure and subsequently its dynamic characteristics. Making use of the measurability of dynamic characteristics, structural damage or deterioration may therefore be inferred from measured changes in dynamics characteristics inversely. The modal properties are important damage indices (Ciambella *et al*. 2011). To make preparations for damage detection, modal properties of the Jiangyin Bridge have been identified from the acceleration data at one-hour interval. The enhanced frequency domain decomposition method is employed for the modal identification. Table 7 summarizes the identified frequencies and shapes of the first 10 modes. It is seen that the frequencies of the bridge are very low. The 1st mode has a frequency of 0.0551 Hz only with a symmetric lateral bending shape. It is also noticeable that the frequencies of the bridge are densely spaced, especially the 1st and 2nd torsional modes. Fig. 20 illustrates the identified shapes of the first 10 modes. The normalized displacement at the locations of 5/8 and 7/8 main span are approximated with the symmetric or anti-symmetric properties of each individual mode.

Table 7 Identified frequencies and shapes of the first 10 modes

Mode No.	Measured frequency (Hz)	Identified shape
1st	0.0551	1st lateral bending (symmetric)
2nd	0.1034	1st vertical bending (anti-symmetric)
3rd	0.1315	2nd vertical bending (symmetric)
4th	0.1445	2nd lateral bending (anti-symmetric)
5th	0.1828	3rd vertical bending (symmetric)
6th	0.1969	4th vertical bending (anti-symmetric)
7th	0.2544	5th vertical bending (symmetric)
8th	0.2624	1st torsion (symmetric)
9th	0.2626	2nd torsion (anti-symmetric)
10th	0.2710	3rd lateral bending (symmetric)

The authors have carried out a detailed investigation into the auto-associative neural network technique for structural damage detection (Zhou *et al*. 2011a). To avoid false-positive or false-negative structural damage alarm due to environmental effects, the authors have also studied the variability of modal frequencies with the back-propagation neural network technique (Ni *et al*. 2007b, Zhou *et al*. 2008, Ni *et al*. 2009, Zhou *et al*. 2010). Based on these studies, a parametric approach for eliminating the environmental effects in vibration-based structural damage detection has been proposed (Zhou *et al*. 2011b). First, a correlation model between damage-sensitive modal frequencies and environmental factors is formulated. With the correlation model, the modal frequencies measured under different environmental conditions are then normalized to an identical reference status of environment so as to eliminate the environmental effects. The normalized modal frequencies are finally applied for structural damage identification. The proposed approach has been verified in the Ting Kau Bridge in Hong Kong. Damages in cables, bearings and girders have been investigated. The results show that this approach is most effective for detecting damage

of a certain severity rather than detecting the onset of damage. The damage becomes detectable when the damage-induced frequency change exceeds 1%. After the verification, the approach has also been embedded in the software system of the upgraded SHM system for the Jianging Bridge. As some design data and drawings of the Jiangyin Bridge are lost, it is difficult to establish a finite element model of the bridge. Therefore, simulation studies of damage detection with this approach are not carried out so far. Damage detection will be performed when an extreme event occurs.

5. Conclusions

In this study, SHM of the Jiangyin Bridge is reported with emphasis on system upgrade and data analysis. First, the upgrade of original SHM system is discussed in detail. Especially, lessons learned from the original SHM system are applied to the design of upgraded system right away. Making use of the long-term structural health monitoring data obtained from the upgraded SHM system, performance assessment is then carried out, including: (i) characterization of temperature profiles and effects. The deck effective temperature and the differential temperature are computed from the temperatures in a deck cross-section for representing the temperature profiles in the deck. After that, the thermal movement of expansion joint is studied and the displacement-temperature correlation model is formulated for design verification as well as extreme displacement prediction. Another temperature effects considered is the temperature-induced strain variability. A linear relationship between strain and temperature is observed and the strain-temperature correlation model has been established for the quantitative estimation of thermal strain; (ii) recognition of wind characteristics and effects. The wind data are analyzed to obtain mean wind speed and direction, wind speed profiles, turbulence intensity, gust factor, and wind spectrum. Verification of design assumptions and rules of thumb are made in the mean while. A linear relationship between transverse wind speed and deck lateral displacement is observed and the correlation model between them has been established for the quantitative estimation of wind-induced deck lateral displacement; (iii) identification of modal properties. Modal properties under normal conditions, including modal frequency and mode shape, have been identified from the acceleration data. Software for structural damage detection with the auto-associative neural network technique has been developed. The results achieved in this study may provide the baseline for structural health evaluation.

Acknowledgements

The authors are grateful to the collaborative partners from the Jiangsu Transportation Research Institute. The work described in this paper was supported in part by a grant from the National Science Foundation of China (Project No. 51208384), a grant from the Science Technology Department of Zhejiang Province, China (Project No. 2012R10071), a grant from the Zhejiang Provincial National Science Foundation of China (Project No. LY12E08009), and a grant from the Research Grants Council of the Hong Kong Special Administrative Region, China (Project No. PolyU 5253/06E).

References

Andersen, E.Y. and Pedersen, L. (1994), *Structural monitoring of the Great Belt East Bridge*, Strait Crossings 94, (Ed. Krokebogr, J.), Rotterdam: Balkema, 189-195.

Barrish, R.A. Jr., Grimmelsman, K.A. and Aktan, A.E. (2000), *Instrumented monitoring of the Commodore Barry Bridge*, Nondestructive Evaluation of Highways, Utilities, and Pipelines IV, (Eds., Aktan, A.E. and Gosselin, S.R.), Bellingham: SPIE, 112-126.

Brownjohn, J.M.W. (2007), "Structural health monitoring of civil infrastructure", *Philos. T. R. Soc. A.*, **365**(1851), 589-622.

Cheung, M.S., Tadros, G.S., Brown, T., Dilger, W.H., Ghali, A. and Lau, D.T. (1997), "Field monitoring and research on performance of the Confederation Bridge", *Can. J. Civil Eng.*, **24**(6), 951-962.

Choi, C.C. (1983), *Wind loading in Hong Kong - commentary on the code of practice on wind effects Hong Kong-1983*, Hong Kong Institution of Engineers, Hong Kong.

Ciambella, J., Vestroni, F. and Vidoli, S. (2011), "Damage observability, localization and assessment based on eigenfrequencies and eigenvectors curvatures", *Smart Struct. Syst.*, **8**(2), 191-204.

Cook, N.J. (1985), *The designer's guide to wind loading of building structures*, Butterworth-Heinemann, UK.

Doebling, S.W., Farrar, C.R. and Prime, M.B. (1998), "A summary review of vibration-based damage identification methods", *Shock Vib.*, **30**(2), 91-105.

Dyrbye, C. and Hansen, S.O. (1997), *Wind loads on structures*, John Wiely & Sons, New York.

Feng, M.Q. (2009), "Application of structural health monitoring in civil infrastructure", *Smart Struct. Syst.*, **5**(4), 469-482.

Fujino, Y. and Siringoringo, D.M. (2011), "Bridge monitoring in Japan: the needs and strategies", *Struct. Infrastruct. E.*, **7**(7-8), 597-611.

Ni, Y.Q., Hua, X.G., Wong, K.Y. and Ko, J.M. (2007a), "Assessment of bridge expansion joints using long-term displacement and temperature measurement", *J. Perform. Constr. Fac.*,**21**(2), 122-135.

Ni, Y.Q., Ko, J.M., Hua, X.G. and Zhou, H.F. (2007b), "Variability of measured modal frequencies of a cable-stayed bridge under different wind conditions", *Smart Struct. Syst.*, **3**(3), 341-356.

Ni, Y.Q., Zhou, H.F. and Ko, J.M. (2009), "Generalization capability of neural network models for temperature-frequency correlation using monitoring data", *J. Struct. Eng. - ASCE*, **135**(10), 1290-1300.

Kim, S., Chang, S.P. and Lee, J. (2002), "Autonomous on-line health monitoring system for a cable-stayed bridge", *Proceedings of the 1st European Workshop on Structural Health Monitoring*, (Ed. Balageas, D.L.), Lancaster: Destech, 1254-1261.

Lau, C.K., Mak, W.P.N., Wong, K.Y., Chan, W.Y.K. and Man, K.L.D. (1999), *Structural health monitoring of three cable-supported bridges in Hong Kong*, Structural Health Monitoring, (Ed. Chang, F.K.), Lancaster: Destech, 450-460.

Maes, M.A., Dilger, W.H. and Ballyk, P.D. (1992), "Extreme values of thermal loading parameters in concrete bridges", *Can. J. Civil Eng.*, **19**(6), 935-946.

Ministry of Transport of the People's Republic of China (2004), *Wind-resistant Design Specification for Highway Bridges*, China Communication Press, Beijing.

Ou, J.P. and Li, H. (2010), "Structural health monitoring in mainland China: review and future trends", *Struct. Health Monit.*, **9**(3), 219-231.

Shi, J.J., Zhang, Q.W. and Xiang, H.F. (2000), "Health monitoring system of Xupu cable-stayed bridge", *Proceedings of the International Workshop on Response and Monitoring of Long Span Bridge*, Hong Kong.

Simiu, E. and Scanlan, R.H. (1996), *Wind effects on structures*, 3rd Ed, John Wiley & Sons, New York.

Sohn, H., Farrar, C.R., Hemez, F.M., Shunk, D.D., Stinemates, D.W., Nadler, B.R. and Czarnecki, J.J. (2004), *A review of structural health monitoring literature: 1996-2001*, Report No. LA-13976-MS, Los Alamos National Laboratory, Los Alamos, New Mexico, USA.

Sumitro, S., Matsui, Y., Kono, M., Okamoto, T. and Fujii, K. (2001), *Long span bridge health monitoring system in Japan*, Health Monitoring and Management of Civil Infrastructure Systems, (Eds., Chase, S.B. and Aktan, A.E.), Bellingham: SPIE, 517-524.

Wong, K.Y. and Ni, Y.Q. (2009), *Structural health monitoring of cable-supported bridges in Hong Kong*, Chapter 12 of the book: Structural Health Monitoring of Civil Infrastructure Systems, (Eds.,V.M. Karbhari and F. Ansari), Woodhead Publishing, Cambridge, UK, 371-411.

Yun, C.B., Lee, J.J. and Koo, K.Y. (2011), "Smart structure technologies for civil infrastructures in Korea: recent research and applications", *Struct. Infrastruct. E.*, **7**(9), 673-688.

Zhou, H.F., Ni, Y.Q. and Ko, J.M. (2007), "A data processing and analysis system for the instrumented suspension Jiangyin Bridge", *Proceedings of the World Forum on Smart Materials and Smart Structures Technology*, (Eds., Spencer, B.F. Jr., Tomizuka, M., Yun, C.B., Chen, W.M. and Chen, R.W.), London: Taylor & Francis, CD-ROM.

Zhou, H.F., Ni, Y.Q., Ko, J.M. and Wong, K.Y. (2008), "Modeling of wind and temperature effects on modal frequencies and analysis of relative strength of effect", *Wind Struct.*, **11**(1), 35-50.

Zhou, H.F., Ni, Y.Q. and Ko, J.M. (2010), "Constructing input to neural networks for modeling temperature-caused modal variability: mean temperatures, effective temperatures, and principal components of temperatures", *Eng. Struct.*, **32**(6), 1747-1759.

Zhou, H.F., Ni, Y.Q. and Ko, J.M. (2011a), "Structural damage alarming using auto-associative neural network technique: Exploration of environment-tolerant capacity and setup of alarming threshold", *Mech. Syst. Signal Pr.*, **25**(5), 1508-1526.

Zhou, H.F., Ni, Y.Q. and Ko, J.M. (2011b), "Eliminating temperature effect in vibration-based structural damage detection", *J. Eng. Mech. - ASCE*, **137**(12), 785-796.

CY